

Document downloaded from:

<http://hdl.handle.net/10251/184839>

This paper must be cited as:

Cerrillo, J.L.; Lopes, C.W.; Rey Garcia, F.; Palomares Gimeno, A.E. (2021). The Influence of the Support Nature and the Metal Precursor in the Activity of Pd-based Catalysts for the Bromate Reduction Reaction. *ChemCatChem*. 13(4):1230-1238.

<https://doi.org/10.1002/cctc.202001797>



The final publication is available at

<https://doi.org/10.1002/cctc.202001797>

Copyright John Wiley & Sons

#### Additional Information

This is the peer reviewed version of the following article: J. L. Cerrillo, C. W. Lopes, F. Rey, A. E. Palomares, *ChemCatChem* 2021, 13, 1230, which has been published in final form at <https://doi.org/10.1002/cctc.202001797>. This article may be used for non-commercial purposes in accordance with Wiley Terms and Conditions for Self-Archiving.

DOI: 10.1002/cctc.202001797

Full Paper

Received: 5. November 2020

Revised: 27. November 2020

## The Influence of the Support Nature and the Metal Precursor in the Activity of Pd-based Catalysts for the Bromate Reduction Reaction.

Dr. Jose<sup>L</sup>. Cerrillo,<sup>[a]</sup> Dr. Christian<sup>W</sup>. Lopes,<sup>[a,b]</sup> Prof. Fernando Rey<sup>[a]</sup> and Prof. Antonio<sup>E</sup>. Palomares<sup>0000-0002-6480-6607\*</sup><sup>[a]</sup>

[a] <orgName/>Instituto de Tecnología Química (CSIC-Universitat Politècnica de València)  
<street/>Camino Vera s.n.  
<city/>Valencia, <postCode/>46022 (<country/>Spain)  
E-mail: apalomar@iqn.upv.es

[b] <orgDiv/>Institute of Chemistry  
<orgName/>Universidade Federal do Rio Grande do Sul  
street missing<?>Avenida Bento Gonçalves, 9500<?>  
postal code missing<?>91509-900<?> <city/>Porto Alegre (<country/>Brazil)

<pict> Supporting information for this article is available on the WWW under  
<url><http://dx.doi.org/10.1002/cctc.202001797></url>

bromate

hydrogenation

palladium

salt precursor

supported catalysts.

**Supported Catalysis:** To prepare an active Pd-catalyst for the bromate reduction reaction in water phase is necessary to use a mesoporous and positive surface charged support that favors reactants interaction with active sites and to select a metal precursor that favours formation of homogeneous and large Pd crystals.

The influence of the support nature and the metal precursor in the activity of Pd-based catalysts for the bromate reduction reaction from @ITQ<?\_>UPVCSIC and @ufrgsnoticias #catalyst

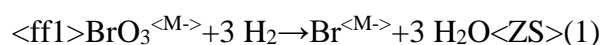
Palladium catalysts supported on different materials (alumina, activated carbon and mixed oxide derived from hydrotalcite) and prepared with different metal precursors (nitrate, chloride and acetate) have been characterized and tested for the bromate reduction reaction. The catalytic behavior depends on the support nature and on the metallic precursor used for the catalyst preparation. Pd catalyst supported on a mixed oxide has a low activity due to the high affinity of the reconstructed support for the  $\text{Br}^{\text{M}}$  formed, preventing the reactants to approximate the active Pd sites. Pd catalyst supported on activated carbon has a surface negative charge and a microporous structure, making difficult the interaction of the active sites with the reactants. The best results are obtained with the catalyst supported on alumina due to its physical-chemical properties, *i.e.* mesoporosity, positive surface charge and reversible adsorption of reactants and products. These characteristics make easy bromate and  $\text{H}_2$  adsorption on the active sites and subsequent reaction, thus resulting in a better activity. The Pd precursor salt also influences the catalytic activity as it has an effect on the Pd nanocrystal size. The best results are obtained with the metal precursor that produces homogeneous and large Pd metallic crystallites.

## Introduction

Environmental catalysis is a sustainable tool for the control of several pollutants. It has been successfully used for the removal of some air pollutants as  $\text{NO}_x$ , VOCs, etc.<sup>[1--7]</sup> Nevertheless the use of catalysis for the control of water pollutants is not easy because for a commercial use, the catalyst must be active at room temperature and atmospheric pressure and must be very stable avoiding metal leaching. Even this, many papers studied the use of catalytic hydrogenation for the control of some water pollutants as halogenated organics, nitrosamines, nitrate, nitrite and bromate.<sup>[8--13]</sup>

Bromate is considered as a mutagenic and carcinogenic agent and for this reason the European Union has established a reference value of  $0.01 \text{ mg/L}$  in drinking water.

It is mainly formed by the oxidation of bromide, usually present in aquatic environments, during ozone or chlorine water disinfection. Some technologies have been proposed in order to minimize this problem such as chemistry reduction, adsorption, photochemical processes, biologic treatments and membranes.<sup>[14--16]</sup> However, none of them are completely effective due to the formation of by-products, to the economic cost or to the waste generation. Catalytic reduction of bromate to bromide can be a sustainable alternative to these methods. Duonghong *et al*<sup>[17]</sup> showed that ruthenium dioxide supported on TiO<sub>2</sub> catalysed the bromate reduction whilst water molecules were oxidised. They studied the pH influence in the reaction and concluded that an acidic pH was necessary in order to increase the reaction rate, but if the pH was too low Br<sub>2</sub> instead of Br<sup>-</sup> was formed. Other authors studied the use of Ru catalysts supported on activated carbon.<sup>[18]</sup> Nevertheless, these catalysts were not active enough for a commercial use, being necessary the addition of a reductant agent as it has been done for the removal of other water pollutant as nitrate.<sup>[19--21]</sup> In this way, the use of hydrogen as a reductant agent can be a good option as it does not modify the quality neither the properties of water:



Different noble metals supported on diverse materials have been studied as catalysts for this reaction<sup>[22--23]</sup> concluding that this technique could be adequate for the removal of bromate in polluted water at room temperature and atmospheric pressure. The use of Pd catalysts supported on carbon nanofibers with a continuous reactor has been reported showing good results even using natural and industrial water polluted by bromate.<sup>[24]</sup> It has been shown that the same catalyst combined with Sn can be used for the reduction of nitrate together with bromate, being both important water

pollutants.<sup>[25]</sup> A cradle-to-gate life cycle assessment study showed the potential of this technology and identified the areas for future optimization of the technology.<sup>[26]</sup>

Recently new papers have described the use in this reaction of mono and bimetallic catalysts supported on activated carbon, titania and zeolites, obtaining interesting results.<sup>[27--34]</sup> The authors have proposed a mechanism for the bromate reduction involving reactions in the liquid phase and on the surface of the catalyst.<sup>[29]</sup> A very interesting review<sup>[13]</sup> describing the use of metallic nanostructures for treating water by degradation of oxyanions has recently appeared, presenting a summary of different catalysts used for the catalytic reduction of bromate.

In this work we study the bromate catalytic hydrogenation at room temperature and atmospheric pressure, using catalysts based on palladium, but supported on different materials (mixed oxide derived from hydrotalcite, activated carbon and alumina) and prepared with different Pd-precursors (nitrate, chloride and acetate). The catalysts have been exhaustively characterized by different techniques as X-Ray Absorption Spectroscopy, XPS, X-Ray Diffraction (XRD), N<sub>2</sub> adsorption/desorption, infrared spectroscopy (IR), CO chemisorption and electron microscopy (SEM, TEM, EDS). The activity of the materials has been related with their physicochemical properties.

## **Results and Discussion**

### **Alumina supported catalysts**

Catalysts supported on alumina with different palladium contents (7, 5, 2.5 and 1<sup>wt.%</sup>) were synthesized using diverse Pd precursors (acetate, nitrate and chloride). The chemical composition and the textural properties of the Pd/Al<sub>2</sub>O<sub>3</sub> catalysts, prepared with PdCl<sub>2</sub> as precursor, are shown in Table<sup>1</sup>. As it can be seen all the materials had a

Pd content close to the established target and a surface area around  $75\text{--}95\text{ m}^2/\text{g}$ . The surface areas of the Pd catalysts were quite similar to that of the support or slightly higher due to the partial modification of the support surface by the highly acidic media used during the metal impregnation.<sup>[35]</sup> The materials presented type II isotherms typical of mesoporous materials. The point of zero charge (pHpzc) of the catalysts was established in 8.9 and consequently they had a positive surface charge under reaction conditions.

XRD patterns of the activated catalysts with different Pd content (Figure<sup>1</sup>) featured the characteristic peaks<sup>[36]</sup> of  $\gamma\text{-Al}_2\text{O}_3$  at  $2\theta=37.5, 39.5, 45.9, 61.0$  and  $66.9^\circ$  and the peaks<sup>[37--38]</sup> assigned to metallic Pd at  $2\theta=40.0, 46.8, 68.3$  and  $82.0^\circ$ . All patterns showed the same peaks but the intensity and the definition of the peaks assigned to Pd (0) rose as the Pd content increased.

The reduced samples were characterized by electron microscopy (FESEM and EDS) in order to determine the catalyst morphology and to analyze the distribution of Pd crystallites on the support. The results showed that the materials had a low crystallinity with a homogeneous dispersion of the palladium species over the support. The dark field scanning-transmission electron microscopy (STEM) allowed determination of the mean particle size of the palladium crystals and the results are shown in Table<sup>1</sup>. Pd was forming nanoparticles without large aggregates and the average crystal size decreased in the same way than the palladium content. Similar results were obtained by CO chemisorption analyses, observing in both cases that Pd dispersion decreased as the metal content increased.

XPS analysis of the sample containing 7% Pd showed the characteristics  $3d_{3/2}$  and  $3d_{5/2}$  Pd peaks (see supplementary material, Figure<sup>S1</sup>). The core level Pd  $3d_{5/2}$  signal only featured one contribution for Pd<sup>0</sup> demonstrating that palladium sites were completely reduced on the catalyst surface.

Figure<sup>2</sup> shows the results obtained for the bromate conversion using catalysts with different palladium content. The selectivity towards bromide was complete in all reactions. As it can be expected, higher reaction rates were obtained when the palladium content was increased.

Catalyst with 7%Pd was the most active one and it was used to check that the reaction rate was not controlled by mass transfer limitations in the reaction conditions. This study was made by changing catalyst loading and stirring velocity. The results are shown in supplementary material (Figures<sup>S2</sup> and <sup>S3</sup>) observing that in our reaction conditions, reaction rate was not controlled by mass transfer limitations.

The use of the turnover frequency (TOF) is necessary for a proper comparison of the catalysts containing different Pd loading. It was calculated as the initial reaction rate (defined as the mols of bromate reacted per time in the linear phase of the reaction) per mol of surface Pd atoms. The last was obtained multiplying the Pd mols by the metal dispersion (this calculated from CO chemisorption analysis, see experimental section). The results are shown in Table<sup>2</sup> and it can be observed that the TOF increased, not linearly, with the Pd content. These results can be related with the formation of crystallites with larger Pd size in the catalyst with higher Pd content (Table<sup>1</sup>). These large nanoparticles favor H<sub>2</sub> activation making easy the H<sub>2</sub> dissociative adsorption due to enhanced solubility of H<sub>2</sub> and formation of β-PdH species.<sup>[40]</sup> This has been observed in many hydrogenation reaction when using Pd catalysts<sup>[23,41--43]</sup> and could explain the highest TOF obtained with the catalyst with the largest Pd mean crystal size. This explanation is appropriate for alumina catalysts where bromate adsorption is not hindered for the existence of a negative surface charge on the catalyst surface, but would not be valid for other type of supports.

The results obtained with the catalysts containing 7% of Pd and prepared with different precursors are shown in Figure<sup>3</sup>.

As it can be observed all the catalysts were very active, reducing completely the bromates before 60 minutes and using only 0.05 g of catalyst, with 100% selectivity towards bromide. Nevertheless, some differences were observed depending on the precursor used for the catalyst preparation. The worst results were obtained with the catalyst prepared with palladium acetate whilst better activity was obtained with the catalysts prepared with nitrate and chloride precursors.

These results can be related again with the different Pd crystal size. TEM analysis of the different materials (Figure 4) showed that the mean Pd particle size of the catalyst prepared from acetate was 7 nm whilst those prepared from nitrate and chloride had a mean particle size of 8–8.5 nm. In these experiments, as it occurred with the catalysts with different Pd loading, the catalyst with the lowest TOF was the one with the lowest mean particle size (Table 3), *i.e.* that prepared with an acetate precursor. On the other hand the best activity was obtained with the catalysts with higher Pd particle size, *i.e.*, those prepared with chloride or nitrate.

The highest activity of the catalyst prepared from a chloride salt was related with a more homogeneous distribution of the crystal size and with the absence of Pd aggregates. This is due to the formation of  $\text{Pd}_x\text{O}_y\text{Cl}_z$  species during the synthesis of the catalyst prepared with  $\text{PdCl}_2$ . As it was discussed in previous papers,<sup>[35,44]</sup> these species were formed during catalyst calcination preventing palladium agglomeration during catalyst activation with hydrogen. After the reduction procedure, the Cl-atoms disappeared and well dispersed Pd nanocrystals were formed.

### **Carbon supported catalysts**

Pd catalysts supported on activated carbon (Pd/AC) were prepared using different palladium precursors (nitrate, acetate and chloride). The main characteristic of the support was its high surface area, around 1100 m<sup>2</sup>/g, with a total pore volume of 0.611 cm<sup>3</sup>/g and



with an average pore width of 2.18 nm (a detailed summary of the textural characteristics of the support can be found in supplementary material, Table S1). These characteristics were not modified after the Pd addition and the catalysts featured a type I isotherm, typical of microporous materials. XPS analysis of the catalyst showed the characteristic  $3d_{3/2}$  and  $3d_{5/2}$  Pd peaks (see supplementary material, Figure S4). The Pd  $3d_{5/2}$  signal core level had two contributions and deconvolution of the peak demonstrated that palladium sites were mainly present as Pd<sup>0</sup> (80%) although some positively charged Pd<sup>2+</sup> (20%) was present in the catalyst.

These materials showed a complete selectivity towards bromide but different bromate conversion was obtained depending on the precursor used. As it can be seen in Figure 5, the best activity was obtained with the catalyst prepared with Pd(NO<sub>3</sub>)<sub>2</sub>, whilst worse results were obtained with Pd-catalysts prepared from acetate and chloride precursors.

As it occurred with the Pd/Al<sub>2</sub>O<sub>3</sub> catalysts, this can be related with the average Pd particle size. In Table 3 is shown that Pd nanocrystals formed on the carbon catalyst prepared from nitrate are twice size of those prepared from acetate or chloride. The comparison of the catalysts supported on carbon show that the highest Pd particle size results in the highest TOF because the first step of the reduction reaction (dissociation of H<sub>2</sub> molecule) was favored with large Pd nanoparticles<sup>[44]</sup> as it was previously discussed.

In order to evaluate the differences obtained in the Pd crystal size depending on the metal precursor used, a XAS study of the different Pd/AC catalysts was made during the different stages of the catalyst preparation.

The analysis of the |FT| of the  $k^2$ -weighted EXAFS during thermal treatment (Figure 6) showed that after reduction at 200°C, the catalyst prepared with palladium chloride still had Cl atoms, although Pd was mainly present as Pd (0). Similar

results were obtained with the catalyst prepared from acetate. In this case after a hydrogen reduction at 200°C some oxygen atoms were close to the Pd atoms. The presence of these nonmetallic atoms located close to Pd sites, avoided the formation of larger Pd particles. This did not occur with the catalyst prepared from nitrate because Pd was completely reduced and all the non-metallic atoms from the precursor were removed during the activation with hydrogen at 200°C. These differences were not observed with the catalysts supported on alumina as they were calcined in air at 450°C, previously to the hydrogen activation, removing in this step all the non-metallic atoms from the different precursors.<sup>[35]</sup>

Nevertheless, the metallic mean particle size of the Pd/AC catalyst prepared with nitrates was even higher than that of the Pd/Al<sub>2</sub>O<sub>3</sub> catalyst prepared with the same precursor but the TOF of the last was much higher than TOF of the Pd/AC catalyst (Table<sup>3</sup>). These results only can be explained by the textural characteristics of the carbon. It has been shown that the high surface area of the support was due to the microporosity of the material, with an average pore width of 2.2 nm. This size is larger than ionic size of bromates, 0.351 nm,<sup>[45]</sup> but this area does not contribute to enhance the catalytic activity as the most active sites are Pd crystallites with a mean size of 4–7 nm (see Table<sup>3</sup>) that cannot be located inside the micropores. On the other hand, this support has a negative surface charge<sup>[46,47]</sup> with a point of zero charge (pHpzc) of 4.5. This makes difficult the bromate adsorption on the carbon surface and this will be the rate limiting step in this type of materials. Consequently these characteristics, microporosity and negative surface charge, resulted in a lower activity of the Pd/AC catalysts compared with those supported on alumina.

### **Hydrotalcite supported catalysts**

The activity in the bromate catalytic hydrogenation of a Pd catalyst supported on a Mg/Al mixed oxide derived from hydrotalcite (Pd-C-Ht) was studied.

This type of catalysts have been described as active materials for many reactions in environmental catalysis<sup>[48--49]</sup> and have been used in a reaction that is quite similar to the bromate hydrogenation, *i.e.* nitrate hydrogenation.<sup>[37,50]</sup> It has been shown that the mixed oxide catalyst formed after calcination of the hydrotalcite has a “memory effect” recovering the hydrotalcite structure when contacted with water because the anions present in the media locate in the interlayer space compensating the positively charged layers. This property favours the interaction of the anionic reactants with the hydrotalcite active sites, resulting in catalysts with improved activity and selectivity. Thus, it can be expected that the same support used for a similar reaction, the bromate hydrogenation, could improve the activity of the Pd-based catalysts.

The catalyst based on a mixed oxide derived from hydrotalcite was prepared with 1<sup>wt.%</sup> of Pd. The support had a high surface area (275<sup>m<sup>2</sup>/g</sup>) that slightly decreased after Pd addition (220<sup>m<sup>2</sup>/g</sup>), being this twice the surface area of the Pd/Al<sub>2</sub>O<sub>3</sub> catalysts. The material had a point of zero charge (pHpzc) of 9.5 and was positively charged under reaction conditions, as the pH of the reaction solution containing the catalyst was 6.9. XPS analysis of the catalyst showed the characteristics 3d<sub>3/2</sub> and 3d<sub>5/2</sub> Pd peaks (see supplementary material, Figure<sup>S5</sup>). The core level Pd 3d<sub>5/2</sub> signal had two contributions, the main for Pd<sup>0</sup> and a small one for PdO, indicating that palladium sites were mainly present as metallic palladium (85%) although some positively charged Pd<sup>2+</sup> (15%) was present in the catalyst.

The material was characterized by XRD and the evolution of the phases formed during the catalyst preparation is shown in Figure<sup>7</sup> (a-c). As it can be seen, prior to calcination (Figure<sup>7</sup>a) some peaks appeared at 2θ=11.2, 22.7, 34.4, 38.4, 45.5, 46.7, 60.1, 61.8 and 65.3° showing the presence of a well-crystallized hydrotalcite phase. After Pd wetness impregnation and subsequent calcination, the XRD pattern evidenced the

presence of a mixed oxide (Figure<sup>7</sup>b), which possesses a typical ill-crystalline MgO-like structure,<sup>[51]</sup> with peaks at  $2\theta=37.0, 43.1$  and  $62.9^\circ$ .

These peaks were slightly shifted if compared with those of periclase, indicating the formation of a Mg-C-Al mixed oxide. After reduction with hydrogen at  $200^\circ\text{C}$ , some small peaks appeared (Figure<sup>7</sup>c) at  $2\theta=37.5, 45.9, 61$  and  $66.9^\circ$ . They were related with alumina indicating a partial segregation of the alumina phase from the mixed oxide. No peaks related with PdO or Pd<sup>0</sup> were observed showing a good dispersion of the metallic phase on the support.

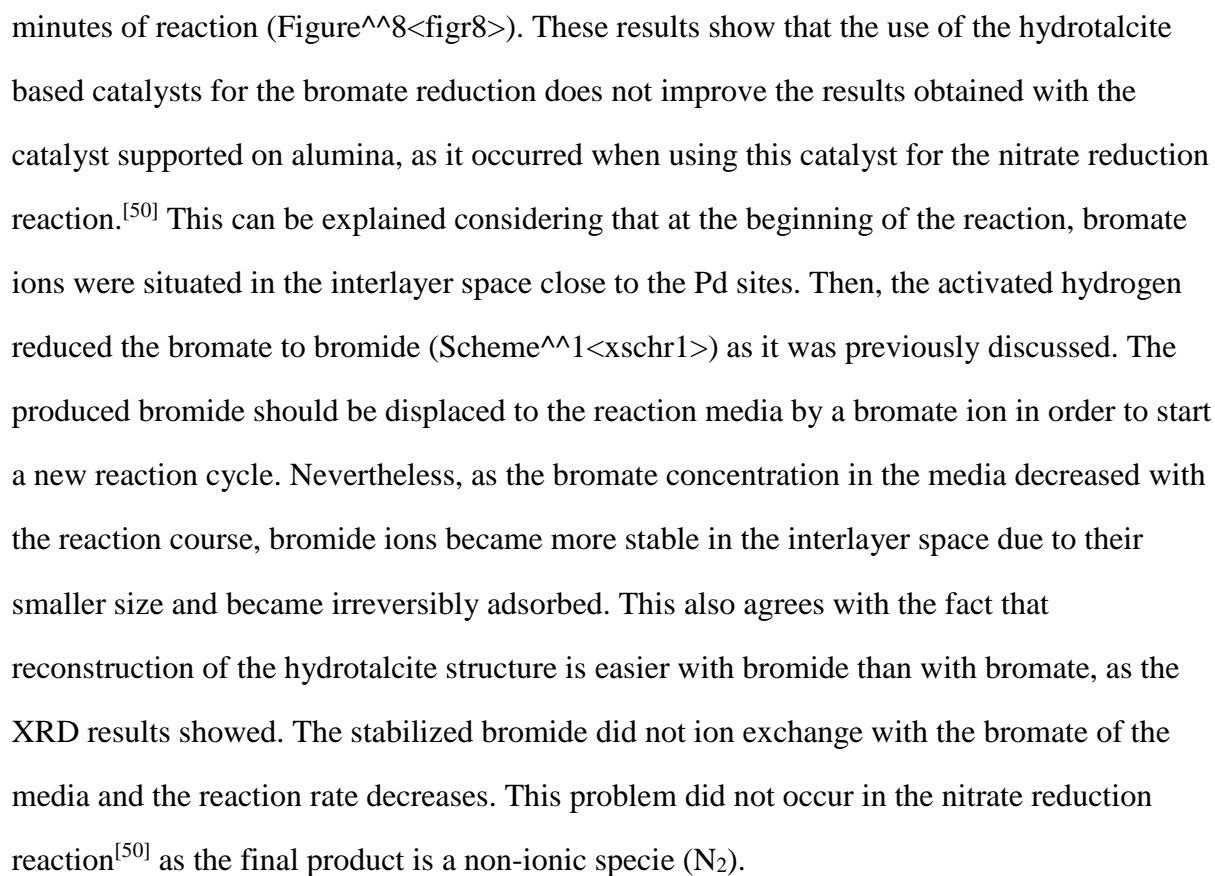
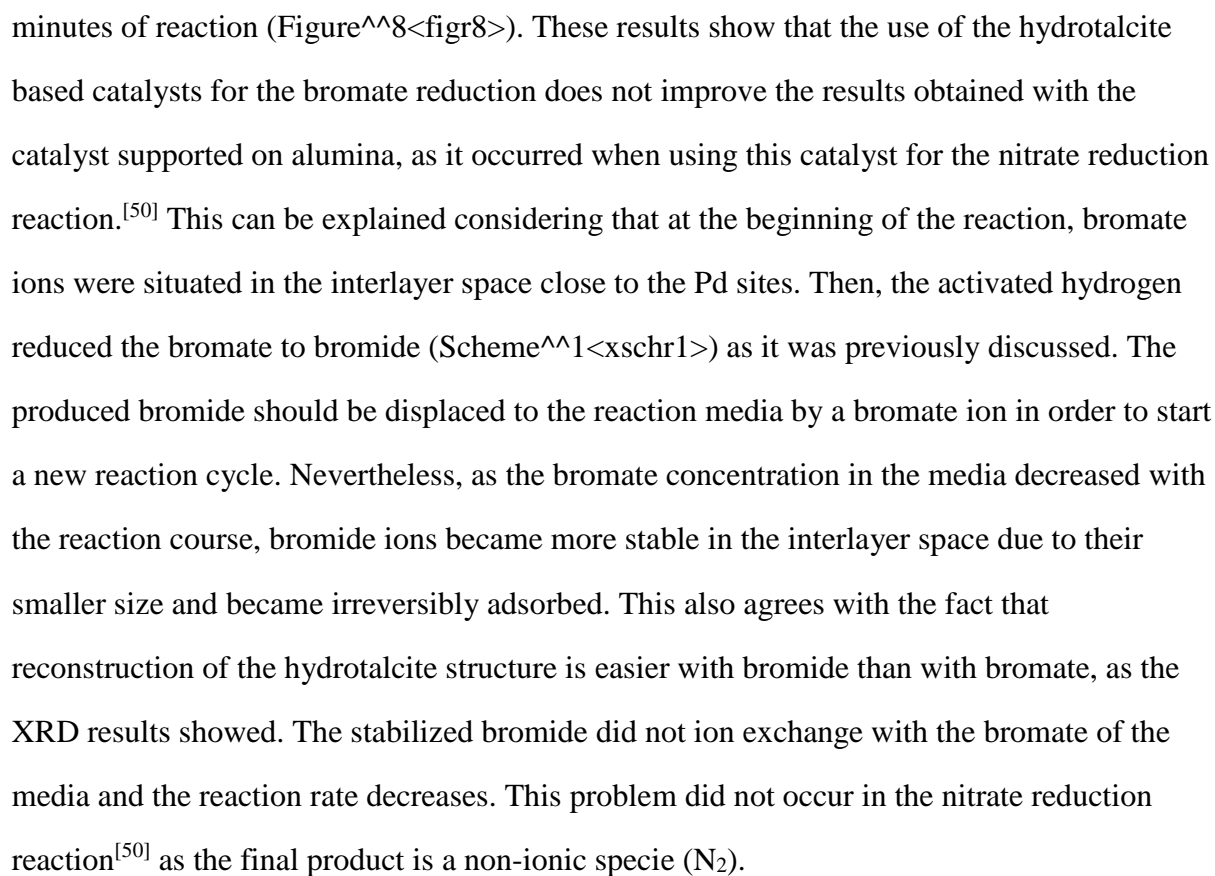
The “memory effect” of this calcined hydrotalcite was also evidenced by XRD. In Figure<sup>7</sup>c was observed that before reaction, the XRD patterns of the sample were those of an ill-MgO like structure, but when the activated catalyst was contacted with a solution containing bromates or bromides, those peaks disappeared, appearing new peaks at  $2\theta=11.2, 22.7, 34.4, 38.4$  and  $60.1^\circ$ , assigned to a hydrotalcite structure. These peaks were more defined when the calcined hydrotalcite was in presence of bromide (Figure<sup>7</sup>e) that when it was in presence of bromate (Figure<sup>7</sup>d). This indicates that the regeneration of the hydrotalcite structure with bromide ions was more effective than its regeneration with bromate ions, probably due to the lower size of Br<sup>M-</sup> if compared with BrO<sub>3</sub><sup>M-</sup>. The lowest size of bromide makes easy the location of these anions in the interlayer space of the hydrotalcite structure.

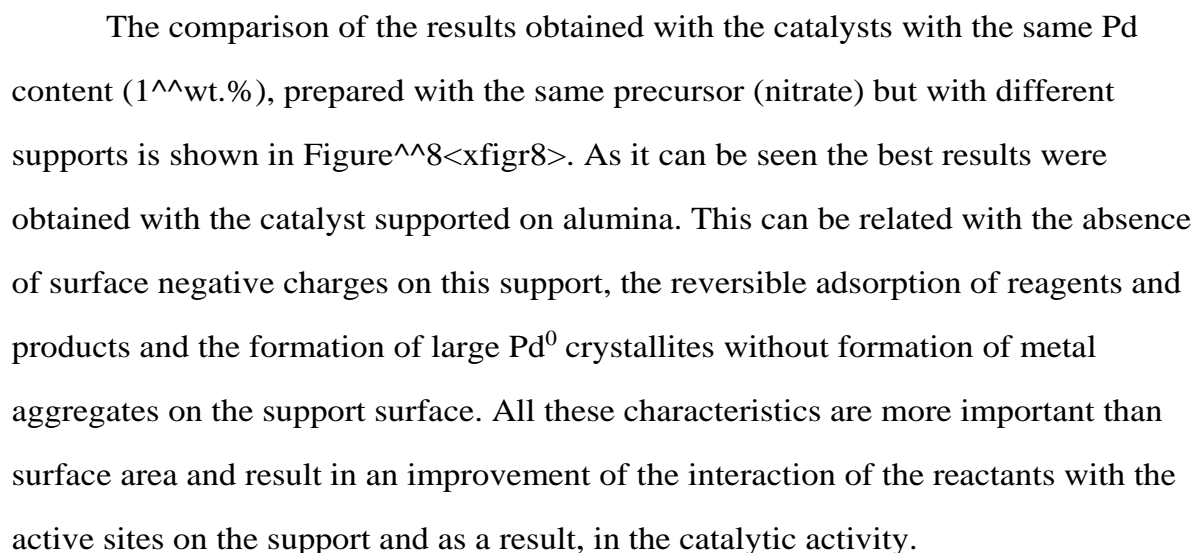
The regeneration of the hydrotalcite phase due to the presence of bromate compensating the positively charged layers was also proved by infrared spectroscopy. The spectrum of the catalyst contacted with the reaction media (supplementary material, Figure<sup>S6</sup>) showed an intense band at  $800\text{ cm}^{\text{M}-1}$  assigned<sup>[52]</sup> to the presence of BrO<sub>3</sub><sup>M-</sup> groups.

Both results evidenced that we can make use of the memory effect<sup>[53]</sup> of calcined hydrotalcite during this reaction. Then, a mechanism was proposed (see Scheme<sup>1</sup>), where the activated catalyst, i.e the mixed oxide containing Pd, when contacted with the reaction media, recovers the hydrotalcite structure due to the location of the bromate in the interlayer space. The bromate would be reduced to bromide by the hydrogen dissociated in the neighbor Pd sites. Since this reduction does not modify the charge of the ions located in the interlayer space, bromide remains in the interlayer space compensating the positively charged layers until they are ion exchanged with the  $\text{BrO}_3^-$  present in the water, starting a new reaction cycle.

In order to check the reliability of the proposed mechanism, the sample was characterized by infrared spectroscopy and XRD, at the beginning and after reaction. The infrared spectra of the catalyst introduced in the reaction media (Figure<sup>S6a</sup>) presented an infrared band at  $1640\text{ cm}^{-1}$  assigned to the bending O-C-H vibration of the water molecules, a band at  $1450\text{ cm}^{-1}$  assigned to the carbonate and a band at  $800\text{ cm}^{-1}$  assigned to bromate. After reaction (Figure<sup>S6b</sup>), the band at  $800\text{ cm}^{-1}$  disappeared, indicating that bromate was reduced to bromide, that did not show infrared bands. This was confirmed by analyzing the XRD of the catalyst after reaction that presented the well-defined patterns of a hydrotalcite phase. These patterns are fully coincident with those shown in Figure<sup>7</sup> corresponding to a mixed oxide derived from hydrotalcite regenerated with a bromide solution, confirming the presence of bromide in the layered structure and therefore the proposed mechanism.

Nevertheless, the catalytic results obtained with this material were worse than those obtained with the catalyst supported on alumina and prepared with the same precursor. The Pd-hydrotalcite needed at least 7 hours of reaction to achieve 80% of bromate conversion, whilst when using alumina with the same Pd content, this conversion was obtained after 50

minutes of reaction (Figure<sup>8</sup>). These results show that the use of the hydrotalcite based catalysts for the bromate reduction does not improve the results obtained with the catalyst supported on alumina, as it occurred when using this catalyst for the nitrate reduction reaction.<sup>[50]</sup> This can be explained considering that at the beginning of the reaction, bromate ions were situated in the interlayer space close to the Pd sites. Then, the activated hydrogen reduced the bromate to bromide (Scheme<sup>1</sup>) as it was previously discussed. The produced bromide should be displaced to the reaction media by a bromate ion in order to start a new reaction cycle. Nevertheless, as the bromate concentration in the media decreased with the reaction course, bromide ions became more stable in the interlayer space due to their smaller size and became irreversibly adsorbed. This also agrees with the fact that reconstruction of the hydrotalcite structure is easier with bromide than with bromate, as the XRD results showed. The stabilized bromide did not ion exchange with the bromate of the media and the reaction rate decreases. This problem did not occur in the nitrate reduction reaction<sup>[50]</sup> as the final product is a non-ionic specie (N<sub>2</sub>).

The comparison of the results obtained with the catalysts with the same Pd content (1<sup>wt.%</sup>), prepared with the same precursor (nitrate) but with different supports is shown in Figure<sup>8</sup>. As it can be seen the best results were obtained with the catalyst supported on alumina. This can be related with the absence of surface negative charges on this support, the reversible adsorption of reagents and products and the formation of large Pd<sup>0</sup> crystallites without formation of metal aggregates on the support surface. All these characteristics are more important than surface area and result in an improvement of the interaction of the reactants with the active sites on the support and as a result, in the catalytic activity.

## Conclusion

From this study can be concluded that it is possible to remove bromate from polluted water by their reduction to bromide using catalysts based on palladium. Nevertheless, it has been shown that the activity depends on three main factors: the support, the palladium precursor and the Pd crystal size. Alumina is better support than carbon due to the absence of microporosity and for its positive charged surface. It is also better than hydrotalcite because alumina does not preferably retain the reaction product on its surface as it occurs with hydrotalcites. The best catalyst was Pd/C- $\rightarrow$ Al<sub>2</sub>O<sub>3</sub> prepared from PdCl<sub>2</sub> because after calcination and reduction, the precursor decomposes completely keeping available all the reduced Pd sites forming large Pd crystallites without the generation of metal aggregates. Then it can be concluded that to prepare an optimum catalyst for this reaction is necessary to select a proper Pd precursor that easily decompose after activation and forms homogeneous large Pd crystallites and, most important, to choose a mesoporous support without negative surface charge and without a preferential adsorption of the reaction products. These characteristics will result in an active catalyst for the hydrogenation of bromates in water phase. Nevertheless it must be taken into account that among those characteristics, formation of large Pd particles will result in a lower metal dispersion and consequently much palladium will be unused, for that reason a compromise between Pd crystal size and metal dispersion is necessary for a commercial use of these catalysts.

## **Experimental Section**

### **Preparation of catalysts**

Catalysts based on alumina were prepared by wetness impregnation of a commercial  $\gamma$ -Al<sub>2</sub>O<sub>3</sub> (Merck) with different Pd precursors, *i.e.* Pd(NO<sub>3</sub>)<sub>2</sub>, PdCl<sub>2</sub> and Pd(C<sub>2</sub>H<sub>3</sub>O<sub>2</sub>)<sub>2</sub>. In order to improve the solubility of the salts, hydrochloric acid was added to the solvent when using palladium chloride and acetic acid when using palladium acetate. After impregnation, catalysts were dried overnight at

100°C and calcined at 500°C. The catalysts were activated with hydrogen at 200°C during 4 hours.

Pd catalysts supported on activated carbon were prepared by wetness impregnation using a commercial activated carbon (Norit GAC 1240W) that was impregnated with different palladium salts *i.e.* Pd(NO<sub>3</sub>)<sub>2</sub>, PdCl<sub>2</sub> and Pd(C<sub>2</sub>H<sub>3</sub>O<sub>2</sub>)<sub>2</sub>. The impregnated support was dried at 100°C and reduced in hydrogen flow at 200°C for 4 hours.

Mg/Al hydrotalcite with a molar ratio of 80/20 was prepared by a standard co-precipitating procedure using two aqueous solutions. The first one contained Mg(NO<sub>3</sub>)<sub>2</sub>·6H<sub>2</sub>O and Al(NO<sub>3</sub>)<sub>3</sub>·9H<sub>2</sub>O with a (Al+Mg) molar concentration of 1.5. The second solution contained NaOH and Na<sub>2</sub>CO<sub>3</sub> in adequate concentration for the total precipitation of aluminium and magnesium and to fix the pH at a value of 13. Both solutions were added simultaneously, while vigorously stirring, at a total flow-rate of 20 mL/h during 4 hours. The gel was aged under autogenous pressure conditions at 60°C for 14 hours, then filtered and washed with distilled water until the pH was 7 and carbonate was not detected in the filtrate. The hydrotalcite was calcined at 550°C in air for 6 hours, obtaining a Mg/Al mixed oxide. Palladium was wetness impregnated on this support using a solution of Pd(NO<sub>3</sub>)<sub>2</sub> following the same procedure described for the catalysts supported on alumina. The catalyst was calcined at 500°C and activated, before reaction, in hydrogen flow at 200°C for 4 h.

### **Characterization**

The chemical composition of the samples was measured by inductively coupled plasma in a Varian 715-ES ICP-Optical Emission Spectrometer.

BET surface areas were determined from the nitrogen adsorption-desorption curves by the conventional multipoint technique with a Micromeritics ASAP 2420. The samples were pretreated at 400°C for 12 hours at high vacuum.



A Philips X'Pert (Cubix)-advance diffractometer coupled to a copper anode X-ray tube operating at 45<sup>^</sup>kV and 40<sup>^</sup>mA was used for the X-Ray diffraction (XRD) characterization.

CO chemisorption was employed to characterize the Pd catalysts supported on alumina. The double isotherm method with a Quantachrome Autosorb-1 equipment was used for this study. Prior to adsorption, the samples were reduced in flowing hydrogen at 200<sup>^</sup>°C for 2<sup>^</sup>h. After reduction, the samples were degassed at 1333<sup>^</sup>Pa for 2<sup>^</sup>h at this temperature and cooled down to 35<sup>^</sup>°C. Then, pure CO was admitted and the first adsorption isotherm was measured. After evacuation at 35<sup>^</sup>°C, the second isotherm was obtained. The difference between total and reversible chemisorbed CO (first and second isotherm) indicated the number of CO molecules that were irreversibly chemisorbed per gram of catalyst (CO molecules linked to Pd atoms). Assuming a Pd/CO atomic ratio stoichiometry of 1, the number of exposed Pd atoms per gram of catalysts on the surface was determined.<sup>[54]</sup> The Pd dispersion was calculated as the fraction of exposed Pd atoms on the catalyst surface compared with the total number of Pd atoms. The average Pd particle diameter was determined assuming a spherical geometry of the metal particles.<sup>[55]</sup>

Field emission scanning electron microscopy (FESEM) was used to obtain catalyst images. The microscopy (ZEISS ULTRA 55, operating at 20<sup>^</sup>kV) has an energy dispersive X-ray equipment system (EDS) for semi-quantitative analysis and mapping of elements. In addition, high resolution transmission electron microscopy (HRTEM) micrographs were obtained with a JEM2100F of 200<sup>^</sup>kV in scanning transmission electron microscopy (STEM) mode. Pd average particle size was obtained by measuring 100 particles at diverse images and positions of the TEM grid. Furthermore, the dispersion of Pd nanoparticles was evaluated by obtaining the volume-area mean diameter that estimates the mean size of these nanoparticles and permits the determination of the dispersion through images of electron microscopy.<sup>[55,56]</sup>

X-ray absorption spectra (XANES and EXAFS) at the Pd K-edge (24350<sup>^</sup>eV) were collected on the CLAES BL22 beamline at ALBA. A Si(311) crystal monochromator, was used to select the

X-ray radiation energy. The measurements were performed in transmission mode and ionization chambers recorded the intensity signal of the incident and transmitted X-ray beam. Pd reference foils were measured in parallel for energy calibration. Other Pd reference compounds were also measured by XAS during the experiment. The samples were *in situ* analyzed with a cell built in our laboratory.<sup>[35]</sup> XAS measurements reproduced the conditions used for the catalyst preparation. EXAFS data analysis were made using standard procedures (software package Viper v. 10.1 for Windows). The spectra pre-edge background was subtracted using a Victoreen polynomial function. The edge jump was normalized to one. The absorption spectra energy threshold was positioned at the first maximum of its derivative. The EXAFS function was evaluated relative to an atomic background estimated with the smoothing spline technique. Radial distribution functions were obtained by Fourier transformation of the  $k^2$ -weighted EXAFS functions. Amplitudes and phases for single and multiple scattering contributions to the EXAFS signal were obtained by applying the FEFF7 code. The fitting was performed in Fourier Transformed  $R$  space (module+imaginary part) between 0.92 and 2.5 Å (when one shell was considered) or between 0.92 and 3.18 Å when two shells were fitted. The results were crossed-checked in  $k$  space (2.98--11.17 Å<sup>-1</sup>). EXAFS refining parameters were maintained as free parameters whilst fulfilling the EXAFS Nyquist theorem. Constraints were imposed to very acute parameter correlations, to unphysical numbers and to the Debye-Waller factor.

X-ray photoelectron spectroscopy (XPS) experiments were collected on a SPECS spectrometer with a Phoibos 150 MCD-9 detector using non-monochromatic AlK $\alpha$  (1486.6 eV) X-ray radiation. The pass energy was 20 eV with an operating pressure of 10<sup>-9</sup> mbar. During the data processing of the XPS spectra, binding energy values were referenced to the C1s peak (BE=284.5 eV). Spectral treatment was performed by using CASA software.

### **Catalytic activity**

The catalysts were tested in a batch stirred tank reactor of 1 L capacity. In this reactor, 600 mL of water containing 50 ppm of bromate were bubbled with pure H<sub>2</sub> during 1 hour. After

that, the catalyst was introduced into the tank and 250 mL/min of H<sub>2</sub> was flowed through the reactor. The addition of the different catalysts resulted in small changes in the pH of the reaction media. The reaction solution had an initial pH of 5.9 that turned into 6.9 after addition of hydrotalcite, into 4.9 after addition of alumina and into 6.2 after addition of carbon catalysts. The experiments were carried out at room temperature and atmospheric pressure. The reactor stirring velocity was 900 rpm. Some experiments were previously made (see supplementary material, Figures S2 and S3) with the most active catalyst, changing stirring velocity and catalyst loading in order to check that in these conditions the reaction rate was not controlled by mass transfer limitations. The reaction progress was followed by acquiring, at defined times, small aliquots for the measurements of reactants (BrO<sub>3</sub><sup>-</sup>) and products (Br<sup>-</sup>). They were analyzed with an ionic chromatograph 883 Basic IC Plus (Metrohm®) equipped with a conductivity detector and a chemical suppression system. The anions were separated using a Metrosep A Supp 5 150/4 column and a Metrosep A Supp 5 150/4 pre-column. The injection volume was 20 μL, the flow rate was 0.7 mL/min and the analysis was made at room temperature. The eluent was an aqueous solution of 3.2 mM Na<sub>2</sub>CO<sub>3</sub> and 1.0 mM NaHCO<sub>3</sub>. A 50 mM H<sub>2</sub>SO<sub>4</sub> solution was used as eluent for the chemical suppressor system.

The Turn Over Frequency (TOF) was defined as the bromate reaction rate (calculated as the mols of bromate reacted per time in the linear phase of the reaction) normalized by the accessible Pd sites that were determined as the Pd total mols multiplied by the metallic dispersion.<sup>[57]</sup>

### Acknowledgements

Authors thank the Spanish Ministry of Economy and Competitiveness through RTI2018-101784-B-I00 (MINECO/FEDER) and SEV-2016-0683 projects for the financial support. We gratefully acknowledge ALBA synchrotron for allocating beamtime and CLÆSS beamline staff for their technical support during our experiment. C.W. Lopes (Science without Frontiers -- Process no. 13191/13-6) thanks CAPES for a predoctoral fellowship. J.L. Cerrillo is grateful to MINECO for the Severo Ochoa contract for PhD formation (SVP-2014-068600). The authors also wish to thank Elena Crespo and Adrián Pla for their collaboration in the experimental part of the paper.

## Conflict of Interest

The authors declare no conflict of interest.

<lit1><jnl>J.<sup>^</sup>J. Spivey, *Ind. Eng. Chem. Res.* **1987**, *26*, 2165--2180</jnl>.

<lit2><jnl>N. Blanch-Raga, A.<sup>^</sup>E. Palomares, J. Martínez-Triguero, M. Puche, G. Fetter, P. Bosch, *Appl. Catal. B* **2014**, *160*, 129--134</jnl>.

<lit3><jnl>D.<sup>^</sup>K. Chlebda, P. Stachurska, R.<sup>^</sup>J. Jedrzejczyk, Ł. Kuteranski, A. Dziedzicka, S. Górecka, L. Chmielarz, J. Łojewska, M. Sitarz, P.<sup>^</sup>J. Jodłowski, *Nanomaterials* **2018**, *8*, 21</jnl>.

<lit4><jnl>L. Chmielarz, M. Jabłońska, *RSC Adv.* **2015**, *5*, 43408--43431</jnl>.

<lit5><jnl>W. Li, J. Wang, H. Gong, *Catal. Today* **2009**, *148*, 81--87</jnl>.

<lit6><jnl>C.<sup>^</sup>M. Vasconcellos, M.<sup>^</sup>L.<sup>^</sup>A. Gonçalves, M.<sup>^</sup>M. Pereira, N.<sup>^</sup>M.<sup>^</sup>F. Carvalho, *Appl. Catal. A* **2015**, *498*, 69--75</jnl>.

<lit7><jnl>B. Li, S. Yuan, *Ceram. Int.* **2014**, *40*, 11559--11566</jnl>.

<lit8><jnl>B.<sup>^</sup>P. Chaplin, M. Reinhard, W.<sup>^</sup>F. Schneider, C. Schuth, J.<sup>^</sup>R. Shapley, T.<sup>^</sup>J. Strathmann, C.<sup>^</sup>J. Werth, *Environ. Sci. Technol.* **2012**, *46*, 3655--3670</jnl>.

<lit9><jnl>M. Hu, Y. Liu, Z. Yao, L. Ma, X. Wang, *Front. Environ. Sci. Eng.* **2017**, *12*, 3</jnl>.

<lit10><jnl>G. Centi, S. Perathoner, *Appl. Catal. B* **2003**, *41*, 15--29</jnl>.

<lit11><jnl>T. Yuranova, C. Franch, A. Palomares, E. Garcia-Bordejé, L. Kiwi-Minsker, *Appl. Catal. B* **2012**, *123*, 221--228</jnl>.

<lit12><jnl>A. López-Gaona, J.<sup>^</sup>A. De<sup>^</sup>los<sup>^</sup>Reyes, J. Aguilar, N. Martín, *React. Kinet. Mech. Catal.* **2010**, *99*, 177--182</jnl>.

- <lit13><jnl>Y.<sup>^</sup>Y. Yin, S. Guo, K.<sup>^</sup>N. Heck, C.<sup>^</sup>A. Clark, C.<sup>^</sup>L. Coonrod, M.<sup>^</sup>S. Wong, *ACS Sustainable Chem. Eng.* **2018**, 6, 11160--11175</jnl>.
- <lit14><jnl>C.-Y. Lai, P.-L. Lv, Q.-Y. Dong, S.<sup>^</sup>L. Yeo, B.<sup>^</sup>E. Rittmann, H.-P. Zhao, *Environ. Sci. Technol.* **2018**, 52, 7024--7031</jnl>.
- <lit15><jnl>M. Naushad, M.<sup>^</sup>R. Khan, Z.<sup>^</sup>A. ALothman, I. ALSohaimi, F. Rodriguez-Reinoso, T.<sup>^</sup>M. Turki, R. Ali, *Environ. Sci. Pollut. Res. Int.* **2015**, 22, 15853--15865</jnl>.
- <lit16><jnl>Y. Zhang, J. Li, L. Li, Y. Zhou, *Environ. Technol.* **2019**, 1--9</jnl>.
- <lit17><jnl>D. Duonghong, W. Erbs, L. Shuben, M. Grätzel, *Chem. Phys. Lett.* **1983**, 95, 266--268</jnl>.
- <lit18><jnl>Z. Dong, W. Dong, F. Sun, R. Zhu, F. Ouyang, *Mechanisms and Catalysis* **2012**, 107, 231--244</jnl>.
- <lit19><jnl>A.<sup>^</sup>E. Palomares, C. Franch, A. Corma, *Catal. Today* **2011**, 172, 90--94</jnl>.
- <lit20><jnl>A. Pintar, J. Batista, J. Levec, *Catal. Today* **2001**, 66, 503--510</jnl>.
- <lit21><jnl>C.<sup>^</sup>L. Constantinou, C.<sup>^</sup>N. Costa, A.<sup>^</sup>M. Efstathiou, *Catal. Today* **2010**, 151, 190--194</jnl>.
- <lit22><jnl>H. Chen, Z. Xu, H. Wan, J. Zheng, D. Yin, S. Zheng, *Appl. Catal. B* **2010**, 96, 307--313</jnl>.
- <lit23><jnl>X. Chen, X. Huo, J. Liu, Y. Wang, C.<sup>^</sup>J. Werth, T.<sup>^</sup>J. Strathmann, *Chem. Eng. J.* **2017**, 313, 745--752</jnl>.
- <lit24><jnl>A.<sup>^</sup>E. Palomares, C. Franch, T. Yuranova, L. Kiwi-Minsker, E. Garcia-Bordeje, S. Derrouiche, *Appl. Catal. B* **2014**, 146, 186--191</jnl>.

- <lit25><jnl>T. Yuranova, L. Kiwi-Minsker, C. Franch, A. E. Palomares, S. Armenise, E. Garcia-Bordeje, *Ind. Eng. Chem. Res.* **2013**, *52*, 13930--13937</jnl>.
- <lit26><jnl>P. Yaseneva, C. F. Marti, E. Palomares, X. Fan, T. Morgan, P. S. Perez, M. Ronning, F. Huang, T. Yuranova, L. Kiwi-Minsker, *Chem. Eng. J.* **2014**, *248*, 230--241</jnl>.
- <lit27><jnl>O. S. G. P. Soares, C. M. A. S. Freitas, A. M. Fonseca, J. J. M. Orfao, M. F. R. Pereira, I. C. Neves, *Chem. Eng. J.* **2016**, *291*, 199--205</jnl>.
- <lit28><jnl>J. Restivo, O. S. G. P. Soares, J. J. M. Orfao, M. F. R. Pereira, *Catal. Today* **2015**, *249*, 213--219</jnl>.
- <lit29><jnl>J. Restivo, O. S. G. P. Soares, J. J. M. Orfao, M. F. R. Pereira, *Chem. Eng. J.* **2015**, *263*, 119--126</jnl>.
- <lit30><jnl>C. M. A. S. Freitas, O. S. G. P. Soares, J. J. M. Orfao, A. M. Fonseca, M. F. R. Pereira, I. C. Neves, *Green Chem.* **2015**, *17*, 4247--4254</jnl>.
- <lit31><jnl>B. J. Restivo, O. S. G. P. Soares, J. J. M. Orfao, M. F. R. Pereira, *Chem. Eng. J.* **2017**, *309*, 197--205</jnl>.
- <lit32><jnl>O. Soares, P. Ramalho, A. Fernandes, J. Órfão, M. Pereira, *J. Environ. Chem. Eng.* **2019**, *7*, 103015</jnl>.
- <lit33><jnl>A. M. Perez-Coronado, O. S. G. P. Soares, L. Calvo, J. J. Rodriguez, M. A. Gilarranz, M. F. R. Pereira, *Appl. Catal. B* **2018**, *237*, 206--213</jnl>.
- <lit34><jnl>M. Li, X. Zhou, J. Sun, H. Fu, X. Qu, Z. Xu, S. Zheng, *Sci. Total Environ.* **2019**, *663*, 673--685</jnl>.
- <lit35><jnl>C. W. Lopes, J. L. Cerrillo, A. E. Palomares, F. Rey, G. Agostini, *Phys. Chem. Chem. Phys.* **2018**, *20*, 12700--12709</jnl>.

- <lit36><jnl>K. Kouachi, G. Lafaye, S. Pronier, L. Bennini, S. Menad, *J. Mol. Catal. A* **2014**, 395, 210--216</jnl>.
- <lit37><jnl>A. Palomares, J. Prato, F. Márquez, A. Corma, *Appl. Catal. B* **2003**, 41, 3--13</jnl>.
- <lit38><jnl>S. Yang, J. Dong, Z. Yao, C. Shen, X. Shi, Y. Tian, S. Lin, X. Zhang, *Sci. Rep.* **2014**, 4, 4501</jnl>.
- <lit39><jnl>J. Sun, J. Zhang, H. Fu, H. Wan, Y. Wan, X. Qu, Z. Xu, D. Yin, S. Zheng, *Appl. Catal. B* **2018**, 229, 32--40</jnl>.
- <lit40><jnl>C. Contescu, D. Macovei, C. Craiu, C. Teodorescu, J.^^A. Schwarz, *Langmuir* **1995**, 11, 2031--2040</jnl>.
- <lit41><jnl>J. Zhou, K. Wu, W. Wang, Z. Xu, H. Wan, S. Zheng, *Appl. Catal. A* **2014**, 470, 336--343</jnl>.
- <lit42><jnl>J.^^A. Baeza, L. Calvo, M.^^A. Gilarranz, A.^^F. Mohedano, J.^^A. Casas, J.^^J. Rodriguez, *J. Catal.* **2012**, 293, 85--93</jnl>.
- <lit43><jnl>M.^^A. Aramendía, V. Boráu, I.^^M. García, C. Jiménez, J.^^M. Marinas, F.^^J. Urbano, *Appl. Catal. B* **1999**, 20, 101--110</jnl>.
- <lit44><jnl>J.^^L. Cerrillo, C.^^W. Lopes, F. Rey, G. Agostini, L. Kiwi-Minsker, A.^^E. Palomares, *Catal. Sci. Technol.* **2020**, 10, 3646--3653</jnl>.
- <lit45><jnl>J.^^A. Wisniewski, M. Kabsch-Korbutowicz, *Environ. Prot. Eng.* **2017**, 43, 189--205</jnl>.
- <lit46><jnl>A.^^G. Gonçalves, J.^^L. Figueiredo, J.^^J.^^M. Órfão, M.^^F.^^R. Pereira, *Carbon* **2010**, 48, 4369--4381</jnl>.

- <lit47><jnl>C.<sup>^</sup>H. Ridaoui, A. Jada, L. Vidal, J.<sup>^</sup>B. Donnet, *Colloids Surf. A* **2006**, 278, 149--159</jnl>.
- <lit48><jnl>C. Mebrahtu, F. Krebs, S. Perathoner, S. Abate, G. Centi, R. Palkovits, *Catal. Sci. Technol.* **2016**, 8 (4), 1016--1027</jnl>.
- <lit49><jnl>P. Marocco, E.<sup>^</sup>A. Morosanu, E. Giglio, D. Ferrero, C. Mebrahtu, A. Lanzini, S. Abate, S. Bensaid, S. Perathoner, M. Santarelli, R. Pirone, G. Centi, *Fuel* **2018**, 225, 230--242</jnl>.
- <lit50><jnl>A.<sup>^</sup>E. Palomares, J.<sup>^</sup>G. Prato, F. Rey, A. Corma, *J. Catal.* **2004**, 221, 62--66</jnl>.
- <lit51><jnl>T. Sato, H. Fujita, T. Endo, M. Shimada, A. Tsunashima, *React. Solids* **1988**, 5, 219--228</jnl>.
- <lit52><jnl>W.<sup>^</sup>A. Alves, R.<sup>^</sup>B. Faria, *Spectrochim. Acta Part A* **2002**, 58, 1395--1399</jnl>.
- <lit53><jnl>F. Cavani, F. Trifiro, A. Vaccari, *Catal. Today* **1991**, 11, 173--301</jnl>.
- <lit54><jnl>A. Martinez, M.<sup>^</sup>A. Arribas, M. Derewinski, A. Burkat-Dulak, *Appl. Catal. A* **2010**, 379, 188--197</jnl>.
- <lit55><book>J.<sup>^</sup>R. Anderson, *Structure of metallic catalysts*, Academic Press, London-New York, **1918**</book>.
- <lit56><jnl>K. Kunimori, T. Uchijima, M. Yamada, H. Matsumoto, T. Hattori, Y. Murakami, *Appl. Catal.* **1982**, 4, 67--81</jnl>.
- <lit57><jnl>M. Boudart, *Chem. Rev.* **1995**, 95, 661--666</jnl>.

Table<sup>^</sup>1      Textural properties, Pd content, average metal particle size and Pd dispersion of the Pd/Al<sub>2</sub>O<sub>3</sub> catalysts prepared with PdCl<sub>2</sub>.<w=3>



	Pd content [wt.%]	BET area [m <sup>2</sup> /g]	External area [m <sup>2</sup> /g]	Pd diameter [nm]	Pd dispersion [%]
Al <sub>2</sub> O <sub>3</sub>	--	80.0	80	--	--
1%Pd/Al <sub>2</sub> O <sub>3</sub>	0.98	75.9	73	2.5 <sup>[a]</sup> /2.1 <sup>[b]</sup>	45.5 <sup>[a]</sup> /39.7 <sup>[b]</sup>
2.5%Pd/Al <sub>2</sub> O <sub>3</sub>	2.57	95.0	86	4.0 <sup>[a]</sup> /3.9 <sup>[b]</sup>	28.3 <sup>[a]</sup> /23.7 <sup>[b]</sup>
5%Pd/Al <sub>2</sub> O <sub>3</sub>	4.99	91.7	78	5.9 <sup>[a]</sup> /5.1 <sup>[b]</sup>	19.0 <sup>[a]</sup> /15.7 <sup>[b]</sup>
7%Pd/Al <sub>2</sub> O <sub>3</sub>	7.15	87.0	77	8.2 <sup>[a]</sup> /8.0 <sup>[b]</sup>	13.7 <sup>[a]</sup> /10.4 <sup>[b]</sup>

[a] Measured by CO chemisorption. [b] Measured by TEM.

Table<sup>2</sup> Reaction rate and TOF calculated for the Pd/Al<sub>2</sub>O<sub>3</sub> catalysts prepared using PdCl<sub>2</sub> as precursor.




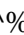
	Reaction rate [BrO <sub>3</sub> <sup>&lt;M-&gt;</sup> mmol/min]	[wt.%] Pd content	[%] Pd dispersion	TOF [min <sup>&lt;M-&gt;1</sup> ]
1%Pd/Al <sub>2</sub> O <sub>3</sub>	8.4 <sup>^</sup> . <sup>^</sup> 10 <sup>&lt;M-&gt;3</sup>	0.98	45.5	3.8
2.5%Pd/Al <sub>2</sub> O <sub>3</sub>	14.1 <sup>^</sup> . <sup>^</sup> 10 <sup>&lt;M-&gt;3</sup>	2.57	28.3	4.1
5%Pd/Al <sub>2</sub> O <sub>3</sub>	20.6 <sup>^</sup> . <sup>^</sup> 10 <sup>&lt;M-&gt;3</sup>	4.99	19.0	4.6
7%Pd/Al <sub>2</sub> O <sub>3</sub>	56.3 <sup>^</sup> . <sup>^</sup> 10 <sup>&lt;M-&gt;3</sup>	7.15	13.7	12.2




Table<sup>3</sup> Average Pd metal [a] particle size (nm) and [b] TOF (min<sup><M->1</sup>) of the 7%wt.% Pd catalysts prepared with different precursors and supported on activated carbon (AC) and alumina.

	Pd(C <sub>2</sub> H <sub>3</sub> O <sub>2</sub> ) <sub>2</sub>	PdCl <sub>2</sub>	Pd(NO <sub>3</sub> ) <sub>2</sub>
7%Pd/Al <sub>2</sub> O <sub>3</sub>	7.0 <sup>[a]</sup> /3.90 <sup>[b]</sup>	8.0 <sup>[a]</sup> /12.20 <sup>[b]</sup>	8.4 <sup>[a]</sup> /11.30 <sup>[b]</sup>

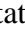
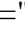
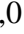
7%Pd/AC	4.5 <sup>[a]</sup> /0.17 <sup>[b]</sup>	4.6 <sup>[a]</sup> /0.27 <sup>[b]</sup>	9.3 <sup>[a]</sup> /1.11 <sup>[b]</sup>
---------	---	---	---

Figure<sup>1</sup> X-ray diffraction patterns of the activated Pd/C-Al<sub>2</sub>O<sub>3</sub> catalysts, prepared using PdCl<sub>2</sub> as precursor with different wt. % Pd content. (a) 1%, (b) 2.5%, (c) 5%, (d) 7%.

Figure<sup>2</sup> Bromate conversion with Pd/Al<sub>2</sub>O<sub>3</sub> catalysts with different wt. % Pd content ( 1%, ( 2.5%, ( 5%, ( 7% (0.05 g of catalyst, 600 mL water with 50 ppm of BrO<sub>3</sub><sup>M-</sup>, PdCl<sub>2</sub> as metal precursor).




Figure<sup>3</sup> Bromate conversion with the 7% Pd/Al<sub>2</sub>O<sub>3</sub> catalysts prepared with different precursors: ( acetate, ( nitrate, ( chloride (0.05 g of catalyst, 600 mL water with 50 ppm of BrO<sub>3</sub><sup>M-</sup>).

Figure<sup>4</sup> TEM images of 7% Pd/Al<sub>2</sub>O<sub>3</sub> catalysts prepared with different precursors: (right) acetate, (middle) nitrate, (left) chloride.

Figure<sup>5</sup> Bromate conversion with 7% Pd/AC catalysts prepared from different precursors: ( acetate, ( nitrate, ( chloride (0.05 g of catalyst, 600 mL water with 50 ppm of BrO<sub>3</sub><sup>M-</sup>).

Figure<sup>6</sup> |FT| of the k<sup>2</sup>-weighted EXAFS spectra of 7% Pd/AC catalysts during thermal treatments. Catalysts prepared with palladium chloride (left), palladium nitrate (middle) and palladium acetate (right).

Figure<sup>7</sup> X-Ray diffraction patterns of hydrotalcite supported Pd catalyst: (a) before calcination, (b) after calcination in air at 500°C (c) after reduction with H<sub>2</sub> at 200°C (d) after activation and in contact with a solution containing bromates or (e) containing bromides.

Figure<sup>8</sup> Bromate conversion with 1% Pd catalysts supported on ( alumina, ( active carbon, ( hydrotalcite (0.5 g of catalyst, 600 mL water with 50 ppm of BrO<sub>3</sub><sup>M-</sup>, PdNO<sub>3</sub> as metal precursor).

Scheme<sup>1</sup> Bromate hydrogen reduction with Pd/C-Ht catalyst.